Journal of Physics and Chemistry of Solids 77 (2015) 122–125

Contents lists available at ScienceDirect

Journal of Physics and Chemistry of Solids

journal homepage: www.elsevier.com/locate/jpcs

Synthesis and characterization of $MnWO_4$ nanoparticles encapsulated in mesoporous silica SBA-15 by fast microwave-assisted method

Luc Huy Hoang [a,*], Pham Van Hanh [a], Nguyen Dang Phu [a], Xiang-Bai Chen [b,c,**], Wu Ching Chou [d]

[a] Faculty of Physics, Hanoi National University of Education, 136 Xuanthuy, Cau Giay, Hanoi, Vietnam
[b] School of Science and Laboratory of Optical Information Technology, Wuhan Institute of Technology, Wuhan 430073, China
[c] Department of Nano Science & Mechanical Engineering and Nanotechnology Research Center, Konkuk University, Chungju 380-701, Korea
[d] Department of Electrophysics, National Chiao Tung University, Hsin-Chu 30010, Taiwan

ARTICLE INFO

Article history:
Received 4 June 2014
Received in revised form
15 October 2014
Accepted 16 October 2014
Available online 22 October 2014

Keywords:
A. Nanostructures
A. Semiconductor
B. Chemical synthesis
C. Infrared spectroscopy (FTIR)
D. Microstructure

ABSTRACT

The $MnWO_4$ nanoparticles encapsulated in mesoporous silica ($MnWO_4$/SBA-15) was successfully synthesized by a fast microwave-assisted method. The products were characterized by X-ray diffraction (XRD), transmission electron microscopy (TEM), nitrogen absorption–desorption isotherm, and Fourier transform infrared spectroscopy (FTIR). Our results showed that the $MnWO_4$/SBA-15 nanocomposites have the ordered hexagonal meso-structure of SBA-15, indicating $MnWO_4$ nanoparticles were successfully distributed into the channels of SBA-15. The size of $MnWO_4$ nanoparticles in SBA-15 is significantly smaller than the size of $MnWO_4$ nanoparticles prepared without SBA-15, indicating that the $MnWO_4$/SBA15 nanocomposites would be very promising for improving photocatalytic activity of $MnWO_4$ nanoparticles.

1. Introduction

$MnWO_4$ has attracted extensive research interests due to its novel multiferroic, electrochemical, ionic properties and its applications in gas sensor, catalyst, electrochromic device, etc. [1–7]. $MnWO_4$ is a narrow band gap semiconductor (Eg~2.8 eV), and is expected to be a new excellent photocatalyst [7]. Recently, encapsulating photocatalytic materials into porous materials such as mesoporous silica, zeolite, carbon fibers or nanotubes has been the subject of extensive studies for enhancing photocatalytic activity [8–11]. Among the photocatalytic support porous materials, mesoporous silica has the advantages of high surface area, adjustable pore size, ordered frameworks and transparent to UV radiation. For various mesoporous silica, SBA-15 with highly ordered hexagonal structure is considered as one prominent photocatalytic support due to its interesting features of high surface area (500–1000 m^2/g), controllable pore diameter (2–30 nm) and high stability [12].

$MnWO_4$ nanoparticles have been synthesized by various methods, including hydrothermal method [4,13], sol–gel method [5], co-precipitation method [6,14], etc. Recently, microwave-assisted method has been widely applied for synthesizing various types of nanoparticles due to the advantages of short reaction time, high reaction rate, energy saving, and easy forming of complex oxides under relative low calcinations temperature [15–17]. In our previous study, we have applied the microwave-assisted method for synthesizing $MnWO_4$ nanoparticles [15]. In this work, we apply the fast microwave assisted method to synthesis $MnWO_4$ nanoparticles encapsulated in mesoporous silica ($MnWO_4$/SBA-15) for its future applications as high efficient photocatalyst. The characterizations of the synthesized $MnWO_4$/SBA-15 nanocomposites indicated that $MnWO_4$ nanoparticles were successfully distributed into the channels of SBA-15. The $MnWO_4$ nanoparticles in the channels of SBA-15 have finer particle size than that synthesized without SBA-15, and the $MnWO_4$ nanoparticles are bonded with SBA-15. These suggest that the $MnWO_4$/SBA-15 nanocomposites would be promising to enhance the photocatalytic activity of $MnWO_4$ nanoparticles.

2. Experimental

The mesoporous silica SBA-15 was prepared using block copolymer Fluroic P123 and Tetraethyl orthosilicate (TEOS), same

* Corresponding author. Fax: +84 4 37547971.
** Corresponding author at: School of Science and Laboratory of Optical Information Technology, Wuhan Institute of Technology, Wuhan 430073, China.
E-mail addresses: hoanglhsp@hnue.edu.vn (L.H. Hoang), xchen@mail.wit.edu.cn (X.-B. Chen).

http://dx.doi.org/10.1016/j.jpcs.2014.10.013
0022-3697/

process as described in Ref. [18]. The synthetic procedure of incorporating $MnWO_4$ nanoparticles into the channels of SBA-15 is carried out as follows. First, SBA-15 was sonicated in solution containing 0.5 M $MnCl_2$ and 0.5 M Na_2WO_4 with the mass ratio of $MnWO_4$: SBA-15 = 90:10. The pH value of the solution was maintained at 7 using NaOH. Then, the solution was placed in a commercial microwave oven (Hitachi Electronic Corp. Japan), and the reaction was performed under microwave power of 300 W for 30 min. The working cycle of the microwave oven was set with 30 s on and 30 s off. The resulted precipitate was separated by centrifugation, washed with deionized water for several times, and dried at room temperature. Finally, the above obtained product was annealed at 600 °C for 4 h. For reference, $MnWO_4$ nanoparticles without SBA15 were prepared with the same process.

Low-angle and wide-angle XRD measurements were carried out using a Siemens D5500 X-ray diffractometer with CuK_α radiation ($\lambda = 1.5406$ Å). TEM images were taken using a JEOL 2010 electron microscope operated at 200 kV. Nitrogen adsorption–desorption isotherms were performed using a TriStar 3000 system. FTIR spectra were obtained using a Nicolet 6700 FT-IR spectrometer.

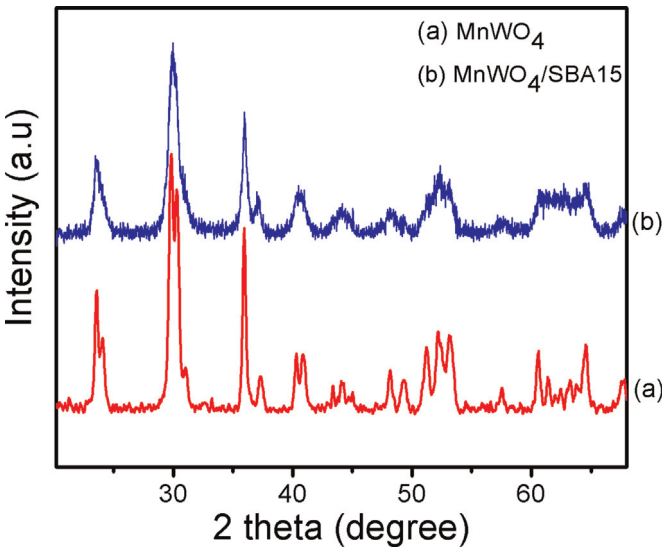

Fig. 2. Wide-angle XRD patterns of (a) $MnWO_4$ nanoparticles and (b) $MnWO_4$/SBA15 nanocomposites.

3. Results and discussion

The low-angle XRD patterns of the SBA-15 and $MnWO_4$/SBA-15 samples are shown in Fig. 1(a) and (b), respectively. The low-angle XRD pattern of the SBA-15 sample exhibits three diffraction peaks. These peaks can be indexed as (100), (110), and (200), which are associated with the *P6mm* hexagonal symmetry of mesoporous structure [12]. The low-angle XRD pattern of the $MnWO_4$/SBA-15 sample shows similar features to that of SBA-15. This indicates that the introduction of $MnWO_4$ nanoparticles into SBA-15 does not collapse the mesoscopic order of hexagonal structure. The main diffraction peak (100) of $MnWO_4$/SBA-15 shifts to higher angle in comparison with that of SBA-15. This would be correlated with the loading of $MnWO_4$ nanoparticles into the mesoporous structure of SBA-15 [19]. Therefore, the low-angle XRD results in Fig. 1 indicate that the $MnWO_4$ nanoparticles are successfully encapsulated in mesoporous silica without collapsing the mesoscopic order of hexagonal structure.

The wide-angle XRD patterns of the $MnWO_4$ nanoparticles and $MnWO_4$/SBA-15 nanocomposites are shown in Fig. 2(a) and (b),

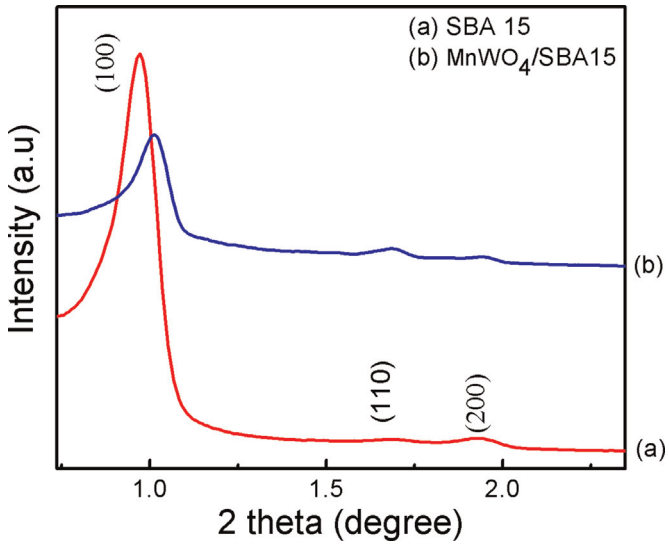

Fig. 1. Low-angle XRD patterns of (a) SBA15 and (b) $MnWO_4$/SBA15 samples.

respectively. All the diffraction peaks of the $MnWO_4$ crystalline phase were detected in the wide-angle XRD patterns of the $MnWO_4$ nanoparticles, indicating good crystalline quality of $MnWO_4$ nanoparticles synthesized by the micro-wave assisted synthesis. The diffraction pattern of the $MnWO_4$/SBA-15 nanocomposites shows similar features to that of the $MnWO_4$ nanoparticles, but with much less resolved peaks. This would be correlated with much smaller particle sizes of $MnWO_4$ nanoparticles in the channels of SBA-15. Using Scherrer's equation, the particle size of the $MnWO_4$ nanoparticles in the channels of SBA-15 is estimated ~5 nm. The particle size of the $MnWO_4$ nanoparticles prepared without SBA-15 is estimated ~15 nm. The much smaller particle size of $MnWO_4$ nanoparticles in SBA-15 is very helpful for enhancing the particle surface area, thus $MnWO_4$/SBA-15 nanocomposites would be very promising to enhance the photocatalytic activity of $MnWO_4$ nanoparticles.

TEM images of the SBA-15 and $MnWO_4$/SBA-15 samples are shown in Fig. 3(a) and (b), respectively. Highly ordered pore array structure of SBA15 is clearly observed in Fig. 3(a). The diameter of the mesopores is ~7 nm. Fig. 3(b) shows that the $MnWO_4$/SBA-15 nanocomposite also has ordered pore array structure, similar as that of SBA15. The better contrast of the TEM image of $MnWO_4$ /SBA-15 nanocomposite would be correlated with the formation of $MnWO_4$ nanoparitlces in the channels of SBA-15. Therefore, TEM images also indicate that $MnWO_4$ nanoparticles are successfully dispersed into the pores of SBA-15, consistent with low-angle XRD results. In addition, Fig. 3(b) does not show clear particle size of $MnWO_4$ nanocrystallines. This indicates that $MnWO_4$ nanoparticles in the channels of SBA-15 would have very fine particle size, consistent with wide-angle XRD result.

The nitrogen adsorption–desorption isotherms of the SBA-15 and $MnWO_4$/SBA-15 samples are shown in Fig. 4(a) and (b), respectively. The isotherm of SBA-15 shows the typical H1-type hysteresis loops of mesoporous materials with two-dimensional hexagonal structure [20]. The isotherm of $MnWO_4$/SBA-15 nanocomposites shows similar behavior comparing with that of SBA-15, but with much smaller hysteresis loop. This suggests that most pores of SBA-15 are filled with $MnWO_4$ nanoparticles. To confirm this, we plotted the pore size distribution curves of the SBA-15 and $MnWO_4$/SBA-15 samples, as shown in Fig. 5. Also, the surface area and pore volume of the SBA-15 and $MnWO_4$/SBA-15 samples are listed in Table 1. As expected, Fig. 5 and Table 1 clearly show that both surface area and pore volume are significantly decreased

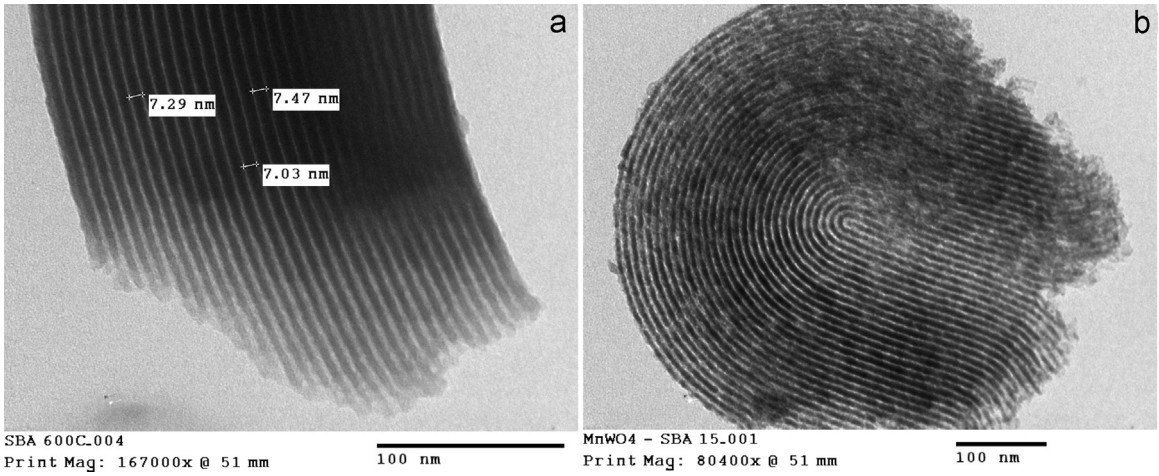

Fig. 3. TEM images of (a) SBA-15 and (b) $MnWO_4$/SBA-15 samples.

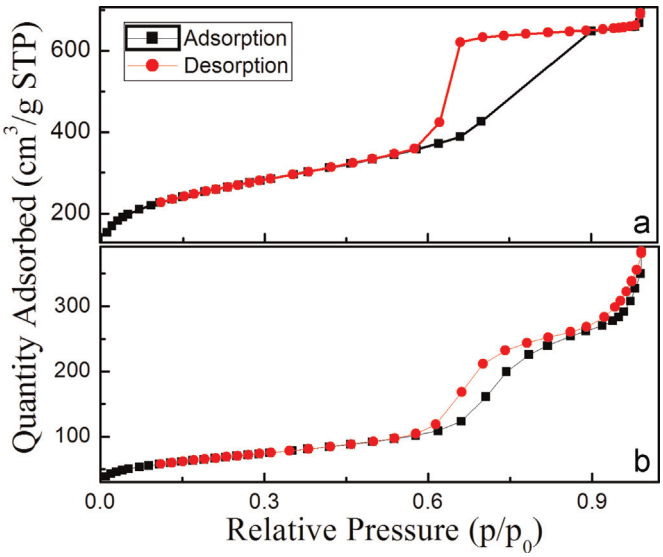

Fig. 4. Nitrogen adsorption–desorption isotherm of (a) SBA-15 and (b) $MnWO_4$ /SBA-15 samples.

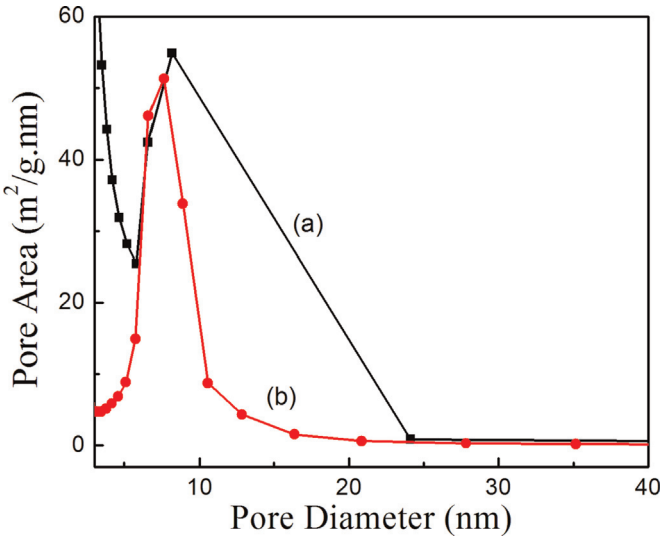

Fig. 5. Pore size distribution of (a) SBA-15 and (b) $MnWO_4$/SBA-15 samples.

when $MnWO_4$ nanoparticles are introduced. This suggests that $MnWO_4$ nanoparticles are successfully dispersed into the pores of SBA-15, consistent with XRD and TEM results.

Fig. 6 shows the FTIR spectra of the SBA-15, $MnWO_4$ nanoparticles and $MnWO_4$/SBA-15 nanocomposites. The band at ~ 1630 cm^{-1} is presented in all three samples, which can be attributed to H–O–H bending vibrations of adsorbed H_2O on the samples [21]. The FTIR spectrum of SBA-15 shows characteristic vibration modes at ~1200, 1080, 970, and 800 cm^{-1} [21–25]. The band at 970 cm^{-1} is correlated with stretching vibrations of free silanol (Si–OH) groups, which can be used an indicator for the bonding of SBA-15 with encapsulated material. The FTIR spectrum of $MnWO_4$ nanoparticles synthesized without SBA-15 shows characteristic vibration modes at ~880, 810, 700, and 590 cm^{-1} [26]. The FTIR spectrum of the $MnWO_4$/SBA-15 nanocomposites not only exhibits the characteristic absorption bands of SBA-15, but also the absorption peaks at 875, 780, and 585 cm^{-1}, which would be correlated with vibration modes of $MnWO_4$ nanoparticles. Note that, for $MnWO_4$/SBA-15 nanocomposites, the peak intensity of 970 cm^{-1} band is much lower than that of SBA-15. This indicates a bonding of $MnWO_4$ nanoparticles with SBA-15, thus the vibration of free silanol groups disappears. In addition, the FTIR of $MnWO_4$ nanoparticles in SBA-15 is quite different with that of $MnWO_4$ nanoparticles without SBA-15 – the peaks at 875 and 585 cm^{-1} are significantly weaker and a peak at 780 cm^{-1} is observed. Maczka et al. [14] showed that for MnWO4 nanoparticles, depending on the morphology and particle size, the IR spectra may differ very strongly; and for small particle size of MnWO4 nanoparticles, a peak at 780 cm^{-1} should be observed. Therefore, the FTIR results also support that $MnWO_4$ nanoparticles of very fine particle size are successfully dispersed into the pores of SBA-15, consistent with XRD, TEM, and nitrogen adsorption–desorption results.

The very fine particle size and the bonding of $MnWO_4$ nanoparticles with SBA-15 would significantly enhance the surface activity of $MnWO_4$ nanoparticles. Thus the $MnWO_4$/SBA15 nanocomposites would be very promising for improving photocatalytic activity of $MnWO_4$ nanoparticles. A systematic study of the photocatalytic

Table 1
Surface area and pore volume of SBA-15 and $MnWO_4$/SBA-15 samples.

Materials	*Specific surface area (m^2/g)*	*Pore volume (cm^3/g)*
SBA-15	908	0,128
$MnWO_4$/SBA-15	236	0,014

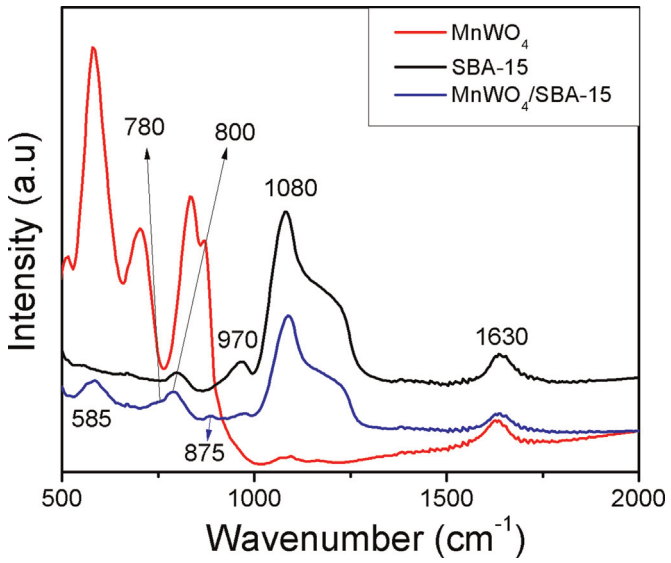

Fig. 6. FTIR spectra of (a) SBA-15, (b) $MnWO_4$, and (c) MnWO4/SBA-15.

activities of the $MnWO_4$ nanoparticles and $MnWO_4$/SBA15 nanocomposites is currently underway. Our experiments indeed show that $MnWO_4$/SBA15 nanocomposites have significantly higher photocatalytic activity than the $MnWO_4$ nanoparticles prepared without SBA15. The details of the photocatalytic activity study will be reported in a later paper.

4. Conclusion

We have successfully synthesized $MnWO_4$/SBA-15 nanocomposites via fast microwave-assisted method. The XRD, TEM, nitrogen absorption-desorption isotherm, and FTIR studies of the $MnWO_4$/SBA-15 nanocomposites showed that the $MnWO_4$ nanoparticles with very fine particle sizes were successfully distributed into the channels of SBA-15. The fine particle size and bonding of $MnWO_4$ nanoparticles with SBA-15 can enhance the surface activity of $MnWO_4$ nanoparticles. Therefore, the $MnWO_4$/SBA-15 nanocomposites would be very promising to enhance the photocatalytic activity of $MnWO_4$ nanoparticles.

Acknowledgements

The authors would like to thank the Vietnam′s National Foundation for Science and Technology Development (NAFOSTED), grant 103.02-2013.51 for financial support.

References

[1] V. Dusastre, D.E. Williams, J. Mater. Chem. 9 (1999) 965.
[2] D.L. Stern, R.K. Grasselli, J. Catal. 167 (1997) 570.
[3] A. Kuzmin, J. Purans, R. Kalendarev, D. Pailharey, Y. Mathey, Electrochim. Acta 46 (2001) 2233.
[4] S. Chen, X.T. Chen, Z. Xue, J.H. Zhou, J. Li, J.M. Hong, X.Z. You, J. Mater. Chem. 13 (2003) 1132.
[5] L. Zhang, C. Lu, Y. Wang, Y. Cheng, Mater. Chem. Phys. 103 (2007) 433.
[6] W.M. Qu, W. Wlodarski, J.U. Meyer, Sens. Actuators B 64 (2000) 76.
[7] H.Y. He, J.F. Huang, L.Y. Cao, J.P. Wu, Desalination 252 (2010) 66.
[8] S. Sun, W. Wang, J. Xu, L. Wang, Z. Zhang, Appl. Catal. B 106 (2011) 559.
[9] W. Guo, F. Zhang, C.J. Lin, Z.L. Wang, Adv. Mater Vol. 24 (2012) 4761.
[10] N. Dubey, S.S. Rayalu, N.K. Labhsetwar, R.R. Naidu, R.V. Chatti, S. Devotta, Appl. Catal., A 303 (2006) 152.
[11] G. Zhang, H. Huang, W. Li, F. Yu, H. Wu, L. Zhou, Electrochim. Acta 81 (2012) 117.
[12] D. Margolese, J.A. Melero, S.C. Christiansen, B.F. Chmelka, G.D. Stucky, Chem. Mater Vol.12 (2000) 2448.
[13] M. Maczka, M. Ptak, A. Pikul, L. Kepinski, P.E. Tomaszewski, J. Hanuza, Vib. Spectrosc. 58 (2012) 163.
[14] M. Maczka, M. Ptak, M. Kurnatowska, L. Kepinski, P. Tomaszewski, J. Solid State Chem. 184 (2011) 2446.
[15] P.V. Hanh, L.H. Hoang, P.V. Hai, N.V. Minh, X.B. Chen, I.S. Yang, J. Phys. Chem. Solids 74 (2013) 426.
[16] S. Ela, S. Cogal, S. Icli, Inorg. Chim. Acta 362 (2009) 1855.
[17] T. Krishnakumar, R. Jayaprakash, N. Pinna, V.N. Singh, B.R. Mehta, A.R. Phani, Mater. Lett. 63 (2009) 242.
[18] D.Y. Zhao, Q. Huo, J. Feng, B.F. Chmelka, G.D. Stucky, J. Am. Chem.Soc. 120 (1998) 6024.
[19] B.J. Aronson, C.F. Blanford, A. Stein, Chem. Mater. 9 (1997) 2842.
[20] Q. Qi, T. Zhang, X. Zheng, L. Wan, Sens. Actuators, B 135 (2008) 255.
[21] J. Ma, L. Li, J. Zou, Y. Kong, S. Komarneni, Microporous Mesoporous Mater 193 (2014) 154.
[22] R.F.S. Lenza, W.L. Vasconcelos, Mater. Res. Vol. 4 (No. 3) (2001) 189.
[23] K. Wang, H. Yang, L. Zhua, J. Liaoa, T. Lua, W. Xing, S. Xing, Q. Lv, J. Mol. Catal. B Enzym. 58 (2009) 194.
[24] O.A. Anunziata, L. Maria Martínez, A.R. Beltramone, Materials 2 (2009) 1508.
[25] H.-M. Kao, J.-D. Wu., C.-C. Cheng, A.S.T. Chiang, Microporous Mesoporous Mater 88 (2006) 319.
[26] S. Saranya, R. Kalai Selvan, N. Priyadharsini, Appl. Surf. Sci. 258 (2012) 4881.